Artificial-Intelligence-Based Methodology for Load Disaggregation at Bulk Supply Point

Yizheng Xu, *Graduate Student Member, IEEE*, and Jovica V. Milanović, *Fellow, IEEE*

***Abstract*—Real-time load composition knowledge will dramatically benefit demand-side management (DSM). Previous works disaggregate the load via either intrusive or nonintrusive load monitoring. However, due to the difficulty in accessing all houses via smart meters at all times and the unavailability of frequently measured high-resolution load signatures at bulk supply points, neither is suitable for frequent or widespread application. This paper employs the artificial intelligence (AI) tool to develop a load disaggregation approach for bulk supply points based on the substation rms measurement without relying on smart meter data, customer surveys, or high-resolution load signatures. Monte Carlo simulation is used to generate the training and validation data. Load compositions obtained by the AI tool are compared with the validation data and used for load characteristics estimation and validation. Probabilistic distributions and confidence levels of different confidence intervals for errors of load compositions and load characteristics are also derived.**

***Index Terms*—Artificial intelligence techniques, confidence level, load disaggregation, probability.**

Nomenclature

AI	Artificial intelligence.
ANN	Artificial neural network.
BP	Backpropagation.
BRBP	Bayesian regulation backpropagation.
CDF	Cumulative distribution function.
CI	Confidence interval.
CL	Confidence level.
DSM	Demand-side management.
GDBP	Gradient descent backpropagation.
LMBP	Levenberg–Marquardt backpropagation.
LME	Load model error.
P	Real power.
PDF	Probability density function.
Q	Reactive oower.
V	Voltage.
WF	Weighting factor.
WFE	Weighting factor error.

Manuscript received December 05, 2013; revised April 02, 2014; accepted July 07, 2014. Date of publication July 31, 2014; date of current version February 17, 2015. This work was supported in part by the EPSRC project Autonomic Power Systems and by EU FP7 Project SuSTAINABLE. Paper no. TPWRS-01556-2013.

The authors are with the Electrical Energy and Power System Group, University of Manchester, Manchester M13 9PL, U.K. (e-mail: yizheng.xu@postgrad.manchester.ac.uk; milanovic@manchester.ac.uk).

Color versions of one or more of the figures in this paper are available online at http://ieeexplore.ieee.org.

Digital Object Identifier 10.1109/TPWRS.2014.2337872

I. Introduction

LOAD compositions forming total demand at network bulk supply point always change due to the inevitable demand variation during the day and season associated with end user operation cycles and habits. This results in the variation of dynamic load characteristics, thus the variation of the dynamic load response to network disturbances. In demand-side management (DSM), a certain amount of demand shifting from the peak time to the off-peak time will help balance generation and demand in the network, however, it will at the same time change the load compositions at bulk supply busses at those periods. The connection of renewable energy devices to the network, particularly at lower voltage levels, will additionally change the load compositions at bulk supply points during the operation of these devices. The change in load compositions at the bulk supply point will further affect its dynamic response to network disturbances and ultimately influence the overall network voltage and angular stability. As a result, being able to predict dynamic load responses to network disturbances at any given time of the day would facilitate efficient active demand management and ensure secure, stable, and economic operation of the power system as a whole. Real-time capture of load composition information will facilitate the real time estimation of dynamic load characteristics and thus benefit DSM and enable close to real time control.

Significant attention was paid to load disaggregation in the past work. Two approaches commonly used for load disaggregation are intrusive load monitoring and nonintrusive load monitoring.

Intrusive load monitoring relies on customer diary record about appliance operation [1], energy data and billing data [2], and, more recently, smart meter data [3]. In intrusive load monitoring, an intermediate monitoring device between the socket and the appliance is installed to record its operation. The customer is additionally required to record the consumption of different appliances in a regular time intervals (i.e., every 30 or 60 min) and keep it as a diary. This approach is inconvenient and expensive for widespread deployment due to the limitation in accessing all appliances in all types of buildings and the vagueness of the customer diary.

Nonintrusive load monitoring relies on the high-resolution load signature measurement data such as current waveform, dynamic load response to a voltage step, instantaneous power, or real power change [4]. There are two types of load signatures, delta form and snapshot form [4]. Delta form load signature is widely used in single-house nonintrusive load monitoring. It uses the change of the power consumption to detect what devices are switched on or switched off [5]. However, this is only suitable for a small-scale area with kilowatt consumption where the watt to kilowatt change is detectable. For a large customer or a bulk supply point with MW to GW consumption, such change is unlikely to be detected by the substation devices. Even if the power change is detected, it is difficult to distinguish the switching of different appliances of the same rating or to distinguish between simultaneous switching of multiple devices and the switching of a single device with the equivalent rating. Snapshot load signature is used for load disaggregation if the high-resolution (faster than 1 Hz) total load signature such as current waveforms, harmonics, or dynamic responses [6] are available at the substation. However, such measurements are not available at the substation under most circumstances, which impedes the frequent and widespread application of the approach.

Considering the deficiency of the past approaches, this paper develops a new load disaggregation approach to estimate the load composition at bulk supply busses based on general substation measurement, i.e., rms of real power (P), reactive power (Q), and voltage (V). It does not require involvement of customers and facilitates real time estimation of dynamic load characteristics at the bulk supply point without carrying out voltage disturbance tests. An artificial intelligence (AI) based algorithm is developed for this purpose, and the artificial neural network (ANN) is adopted as the AI tool. By classifying the customers into different categories [7]–[11] and making use of the appropriate voltage-dependent load models for different load categories, the algorithm captures the relationships among the voltage, real and reactive power consumptions, and appropriate weighting factors of the load categories. The weighting factors are assigned to different load categories by considering all possible load category combinations (i.e. 0% to 100%) under all possible power system normal operation voltages (i.e., 0.9 to 1.1 p.u). Monte Carlo simulation is used to generate the weighting factors for load composition within the total load and bus voltages and to establish P and Q of the total load based on individual contributions of different load categories. The inputs to the ANN in the training process are the voltage and the total load P and Q, and the targets are the weighting factors (WFs) of different load compositions. The error between the calculated WFs and the WFs obtained from validation data is assessed and its probability density function (PDF) and the confidence level (CL) of different confidence intervals are calculated. The estimated WFs are then used as an input to estimation of aggregate load characteristics and the results are compared with the validation data.

II. Artificial Neural Network

An ANN is an interconnected assembly of simple processing elements, units or nodes, whose functionality is based on the animal neuron. The processing ability of the network is stored in the inter-unit connection weights, obtained by a process of adaptation to a set of training patterns. It is inspired by biological nervous system and now widely applied to number of areas such as load prediction [12]–[14], curve fitting [11] and clustering [15]–[17]. A two-layer feed-forward ANN (FFANN) is employed in this study because of its simple structure and potential ability to represent almost all input-output relationships with a finite number of discontinuities as long as an appropriate size is assigned to the hidden layer [17].

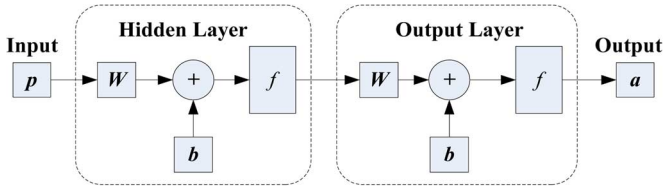

Fig. 1. Structure of an FFANN.

A. Structure

The structure of a two-layer FFANN with a hidden layer and an output layer is shown in Fig. 1. Either of the layers contains an input vector $\boldsymbol{p}$, a weight matrix $\boldsymbol{W}$, a bias vector $\boldsymbol{b}$, a sum operator, a transfer function (TF) f, and an output vector $\boldsymbol{a}$. The weighting matrix weighs the input elements, the bias vector biases the weighed inputs via the sum operator, the sum operator gathers the weighed inputs and the biases to produce an intermediate variable for the TF, and the TF produces the final output of the layer. The input–output relationship in either layer can be represented by

$$\boldsymbol{a} = f(\boldsymbol{W}^T\boldsymbol{p} + \boldsymbol{b}) \tag{1}$$

and the output of the hidden layer is the input of the output layer. Further theoretical background on ANN operation mechanism can be found in, e.g., [12], [17], and [18].

B. Main Parameters Configuration

1) Hidden Layer Size: In [19], a novel approach is proposed to optimize the number of neurons in the hidden layer to avoid over-fitting. Mathematical approximation for $N/d \gg 30$ is shown in

$$n = \sqrt{\frac{N}{d \ln N}} \tag{2}$$

where n is the number of neurons in the hidden layer, N is the number of the training set, and d is the input dimension. If N/d is smaller or close to 30, optimal n most frequently occurs on its maximum. In [20] and [21], a signal-to-noise-ratio figure (SNRF) and a genetic algorithm are proposed to optimize the size of hidden layers, respectively, which both prove that, although the hidden layer size is always finally determined by trial and error with different numbers around the estimation of (2), the nearest integral to the estimation of (2) works well under most circumstances.

2) Transfer Function: The transfer function (TF) could be any differentiable function. The most commonly used TFs are log-sigmoid $(logsig)$, tan-sigmoid $(tansig)$, and linear transfer

function ($purelin$) [17]. The output ranges of the three TFs are, respectively, [0,1], [−1,1] and $[-\infty, +\infty]$, and the input range is $[-\infty, +\infty]$ for each of them.

3) Training Algorithm: Backpropagation (BP) [18] is widely used in ANN training. It has different variations, such as most commonly used gradient descent backpropagation (GDBP), Levenberg–Marquardt backpropagation (LMBP), and Bayesian regulation backpropagation (BRBP). GDBP is also called the basic BP, in which the weights are moved in the direction of the negative gradient. LMBP is widely adopted as the training algorithm due to its fast speed and high performance accuracy [17]. Since the fast speed of LMBP induces relatively large uncertainties and instability, a BRBP is sometimes employed to increase the robustness and stability of ANN, despite its slower processing speed than LMBP. BRBP updates the weight and bias based on Levenberg–Marquardt optimization. It minimizes a combination of squared errors and weights and determines the correct combinations in order to produce a network that generalizes better [17]. It generally works the best, especially when the network inputs and targets are scaled so that they fall approximately in the range [−1,1].

III. Load Model

The term "load model" denotes an analytical, mathematical, equivalent-circuit-based, physical-component-based, or otherwise established or formulated representation of a load, which correctly represents the changes in real and reactive power demands of the modeled load as a function of certain power system parameter (i.e., voltage or frequency) variations. An exponential load model describing dependence of real power (P) on voltage and frequency is given by

$$P = P_0 \left(\frac{V}{V_0}\right)^{k_{pu}} \left(\frac{f}{f_0}\right)^{k_{pf}} \tag{3}$$

where k_{pu} and k_{pf} are the voltage and the frequency exponent, respectively. Similar relationship applies to Q.

Generally, during normal operation of power system, the voltage may vary within ±10% and the frequency within ±0.2 Hz (i.e., ±0.4% for a 50 Hz system). In some special cases with extremely light load, the tolerance of the frequency change might go up to ±1%. According to [11], which is one of the most recent and most comprehensive reference on the subject, the values of frequency exponents (for both P and Q) for different types of individual loads generally lie between −4.5 and 5 (e.g., agriculture pump and TV sets are some of devices with extreme values of frequency exponents). Further details are available in [11]. Considering the weightings of different load types in load mix at the bulk supply point, the average value of the frequency exponent of the aggregate load will be closer to 0 than the frequency exponents of the individual devices which may attain some larger. Since the frequency variations in the system are much smaller (almost an order of magnitude) and less frequent than voltage variations, load dependence on frequency is generally neglected, except in specific frequency regulation and frequency stability studies. In this study, load dependence on frequency is neglected as the inclusion of frequency dependency in load models would require more variables to be calculated (i.e., frequency exponents for both real and reactive power). This significantly increases memory and processing time requirements without bringing sufficient (if any) improvement in accuracy of the results of load disaggregation, which are the focus of this research.

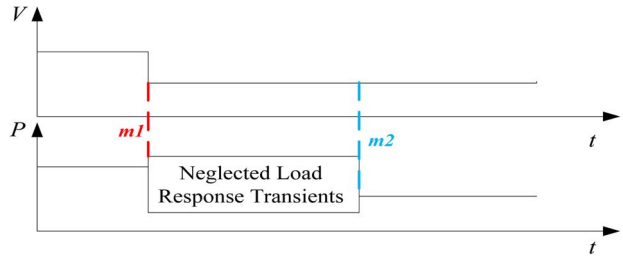

Fig. 2. Neglected transient processes between two measurements $m1$ and $m2$.

Since the methodology developed in this study relies on steady state measurements of real and reactive power and the voltage at the bus, only static load models are considered. They ultimately describe the demand composition. The transient processes, i.e., the dynamic characteristics of the response of the real and reactive power (the area between points $m1$ and $m2$ in Fig. 2) which occurs between two steady-state values is not considered in this study.

A. Most Commonly Used Load Models

The recently conducted international survey by CIGRE WG C4.605 on industrial practice on load modeling [22] found that 70% of 95 surveyed utilities and system operators around the world use only static load model for power system stability studies. The most commonly used types of static load models are a voltage-dependent exponential load model, shown as

$$P = P_0 \left(\frac{V}{V_0}\right)^{\alpha} \tag{4}$$

for real power, and a ZIP model [11]. A similar relationship to the one shown in (4) applies to reactive power. For some models, some other parameter (e.g., capacitance or inductor) or terms with exponents other than 0, 1, or 2 are needed, thus the general form of voltage-dependent polynomial load model can be written as a function of voltage and other parameters and is shown as

$$P = f_P(V, \text{Para}) \tag{5}$$

$$Q = f_Q(V, \text{Para}). \tag{6}$$

In (4)–(6), P is the actual real power, Q is the actual reactive power, V is the actual load supply voltage, P_0 is the initial real power, V_0 is the initial load supply voltage, α is exponential model coefficients for real power, and Para represents other parameters.

From [11], it is known that the exponential model coefficients are much more voltage-dependent than ZIP model or polynomial model coefficients. The load modeling result in [7] shows that, under most circumstances, an exponential load model with a constant coefficient performs less accurately than a ZIP or polynomial with constant coefficients within the same voltage range. However, for most case studies, an exponential load model is much more convenient than a polynomial model

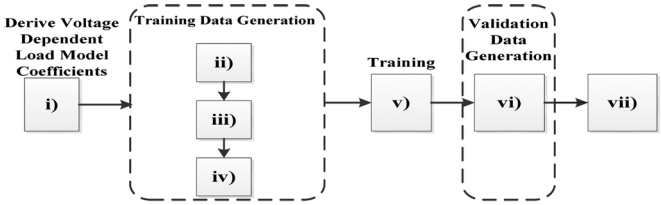

Fig. 3. Flowchart of the proposed methodology.

and a ZIP model because it contains only one term and only one parameter for either P or Q. As a result, it is necessary to obtain the relationship between the exponent and the voltage if an exponential load model is adopted.

B. Aggregate Load Models

As power system load consists of different load categories, and if the composition of each load category is known, via component-base load modeling approach, the aggregate load can be represented by weighed average of individual load, shown as

$$P_{\text{Agg}} = \sum_{i=1}^{N} w_i P_i \tag{7}$$

where P_{Agg} is aggregate load real power consumption in per unit, w_i is the weighting factor for load category i, P_i and Q_i are actual real and reactive power consumption of load category i in per unit, and N is the total number of load categories. Similar relationship applies to reactive power. The weighting factors are the percentages of different load categories participating in the bulk supply point. This relationship will be used in the load disaggregation in following sections.

IV. Methodology and Data Processing

The AI-based load disaggregation approach considers all possible combinations of load supply voltage and load compositions at the bulk supply point and captures the relationship among the load compositions, the bulk supply point V, P, and Q under all circumstances via offline training.

The approach can be summarized into the following steps: i) derive voltage-dependent P and Q exponential load model coefficients for different individual load categories; ii) generate random voltages and weighting factors for training; iii) derive all combinations of voltages and weighting factors; iv) use the result in 1) and 3) to define the input and the target for the ANN; v) train ANN and save trained ANN; vi) repeat ii)–iv) to generate validation data; and vii) validation, probability distribution derivation, and CL analysis. A flowchart of the proposed methodology is shown in Fig. 3. Further details are described in the following subsections.

A. Voltage-Dependent Exponential Model Coefficient

To make the programming process easier and to illustrate the methodology, the exponential load model is selected in this study. As the exponential model coefficient is voltage-dependent, P and Q exponent–voltage relationship for each load category should be derived before the model is applied to load disaggregation. Exponents under different voltage can be calculated using (4), ideally with adequate field measurement data (i.e., $P\&Q\&V$ sets). If the field measurement data are not available, the more accurate polynomial or ZIP model can be used alternatively as the "filed measurement data". The relationship between P exponent and the supply voltage in both cases ($V \neq V_0$) can be calculated from

$$\alpha(V) = \frac{ln\left(\frac{P_{\text{measurement}}}{P_0}\right)}{ln\left(\frac{V}{V_0}\right)} \quad \text{or} \quad \alpha(V) = \frac{ln\left[\frac{f_P(V,\text{Para})}{\text{P}_0}\right]}{ln\left(\frac{V}{V_0}\right)} \tag{8}$$

where α is exponential model coefficient for real power, $P_{\text{measurement}}$ is field measurement data of P, V is the actual load supply voltage in per unit, V_0 is the initial load supply voltage in per unit, and Para represents other parameters. Similar relationship applies to reactive power exponent $\beta(V)$.

In a component-based approach [11], loads are classified into different load categories according to their load characteristics. In this study, loads are classified into eight categories [7]–[11], including:

1) lighting (L);
2) SMPS (switch mode power supply);
3) rectifier (REC);
4) residential cold load (CL);
5) residential wet load (WL);
6) resistive load (R);
7) three-phase constant torque induction motors (CTIM3);
8) three-phase quadratic torque induction motors (QTIM3).

Types 4) and 5) are single-phase quadratic torque induction motors (QTIM1) and single-phase constant torque induction motors (CTIM1), respectively. Types 7) and 8) are typically used in commercial and industrial load sectors. The polynomial load models for different load categories used in this study are listed in Table I. The models were originally developed and validated through laboratory measurements [7]–[10]. All values of parameters in Table I are in per unit. In the model of lighting load (L), $P_b = 1$ is the base power [10], $P_0 = 1$ p.u., and Q_0 depends on the nominal power factor. The exponent-voltage relationships for SMPS, wet load, and CTIM3 are shown in Fig. 4,

TABLE I
Load Models of Different Load Categories Used in This Study

Load Type		Mathematical Model
L	P	$P=0.581+0.371\times V-0.0151\times P_b+0.037\times V^2$ $+0.016\times V\times P_b-2.457\times 10^{-6}\times P_b^2$
	Q	$Q=1.193+1.604\times V-0.0108\times P_b$ $+1.119\times V^2-0.045\times V\times P_b-4.441\times 10^{-4}\times P_b^2$
SMPS	P	$P=P_0$
	Q	$Q=Q_0\times(0.029\times V^2+0.188\times V+0.272+0.236\times V^{0.033}+0.236\times V^{0.033})$
REC	P	$P=4.6902\times V^2-6.7404\times V+2.3222-0.85852\times P_0+1.8969\times P_0\times V$
	Q	$Q=Q_0\times(0.266\times V^2+0.1641\times V-0.042+0.234\times V^2+0.234\times V^2)$
CL	P	$P=0.101\times V+0.099\times V^2+0.798$
	Q	$Q=-0.905\times V+1.402\times V^2+0.503$
WL	P	$P=-0.634\times V+0.268\times V^2+1.366$
	Q	$Q=-0.905\times V+1.402\times V^2+0.503$
R	P	$P=P_0\,(V/V_0)^2$
	Q	$Q=0$
CTIM 3	P	$P=-0.634\times V+0.268\times V^2+1.366$
	Q	$Q=-2.15\times V+1.751\times V^2+1.4$
QTIM 3	P	$P=0.424\times V-0.147\times V^2+0.724$
	Q	$Q=-2.15\times V+1.751\times V^2+1.4$
P_b is the base power		

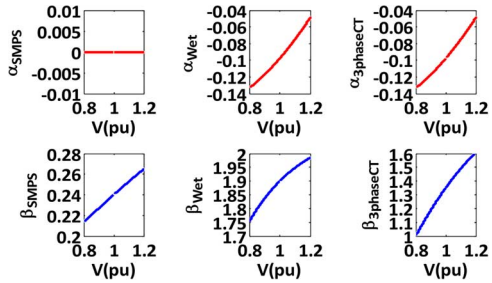

Fig. 4. P and Q exponent–voltage relationship of different load categories.

Exponent–voltage relationships of other load categories are not shown due to the space limitation.

Once obtained, the relationship is stored in an ANN for further use. With these relationships, actual P and Q in per unit for individual load categories under different load supply voltage can be calculated from (4).

B. Training Data Generation

1) Voltage Data Generation: In most cases, the power system is under normal operation, with the bus voltages ranging from 0.9 to 1.1 p.u. Considering the potential margins in extreme cases, the voltage range used in this study is [0.85, 1.15] p.u. By using Monte Carlo simulation, voltages ranging from 0.85 to 1.15 p.u are generated randomly via uniform distribution, ensuring that all voltages are sampled with equal probability for training. The number of voltage samples is denoted as N_V.

2) Weighting Factor Generation: In Section IV-A, it was shown that, in this study, there are a total of eight load categories. To ensure that all of the possibilities are considered and generated, the eight categories are further split into two parts, the dynamic part and the static part, and both parts changed gradually. The dynamic part contains four types of motor loads, the residential cold load (QTIM1) and wet load (CTIM1), commercial and industrial induction motors (QTIM3 and CTIM3), and the static part includes lighting, SMPS, rectifier, resistive load. The dynamic part contribution to total load is varied gradually from 0% to 100% with a step of 5%, and the static part changes correspondingly to make up 100%. There are in total 21 possibilities of such dynamic-static percentage combination.

For each of the 21 possibilities, the WFs of different load categories are generated randomly via uniform distribution within corresponding parts. For example, for a 20% dynamic and 80% static combination, the WFs of the motor loads which make up the dynamic part are generated from 0% to 20%, with a sum of 20%, and similarly, the WFs for all the static loads which make up the static part are generated from 0% to 80%, with a sum of 80%. All of the WFs generated are positive. The number of WFs generated for each of the 21 dynamic-static combination possibilities is denoted as N_W.

3) Combinations of Voltage and Weighting Factor: After random voltages and WFs are generated, all possible combinations of voltages and weighting factors are obtained in order to generate the inputs for ANN. There are in total $N_V \times 21 \times N_W$ V-WF combinations.

4) ANN Input and Target: For each combination of V and WF, the total real and reactive power at the bulk supply point can be calculated by (7). They can be regarded as the measurement (rms value) from the bulk supply point. The real and reactive power in (7) for individual load categories under different voltages can be calculated with the exponent–voltage relationship obtained in Fig. 4, (8), (4), and (7). The inputs for ANN are total load real power P_{Agg}, total load reactive power Q_{Agg}, and supply voltage V at the bulk supply point, and they are written in an input matrix ***PTRN*** represented by

$$\boldsymbol{PTRN} = \begin{bmatrix} P_{Agg,1} & \cdots\cdots & P_{Agg,N_V\times 21\times N_W} \\ Q_{Agg,1} & \cdots\cdots & Q_{Agg,N_V\times 21\times N_W} \\ V_1 & \cdots\cdots & V_{N_V\times 21\times N_W} \end{bmatrix}. \quad (9)$$

Sometimes, when the Q measurement is not available, the inputs for ANN become P and V only, and the second row of (9) is removed. The targets of ANN are corresponding WF used to calculate aggregate real and reactive power, written as a target matrix ***TTRN*** represented by

$$\boldsymbol{TTRN} = \begin{bmatrix} w_{1,1} & \cdots\cdots & w_{1,N_V\times 21\times N_W} \\ \vdots & \vdots\ w_{i,j}\ \vdots & \vdots \\ w_{8,1} & \cdots\cdots & w_{8,N_V\times 21\times N_W} \end{bmatrix} \quad (10)$$

where $w_{i,j}$ is the WF of load category i for jth V-WF combination, with $1 \le i \le 8$, $1 \le j \le N_V \times 21 \times N_W$. All data in input matrix and target matrix are in per-unit values.

C. Training

After the input and the target are defined, an ANN is employed as the training tool. The size of the ANN hidden layer is configured as the nearest integration to the estimation of (2). The TF for the hidden layer and the output layer are configured as $logsig$ and $tansig$, respectively, to ensure that the output of the ANN (i.e., the WFs) is within [0,1]. (Note: as the output of a $logsig$ function is insensitive to its input, if selected as the TF of the output layer, it will restrict the final ANN output to a quite small range that is not able to cover the range of the weighting factors. Therefore, the best way is to use a $tansig$ TF, with positive inputs to the output layer. To ensure the inputs of the output layer (also the output of the hidden layer) are positive, a $logsig$ is selected as TF for the hidden layer.).

ANN training can be either dynamic training or one-time training. In dynamic training, the response of the trained ANN is not only dependent on the input at the current time, but also depends on the history of the input sequences. Dynamic training is widely used in time-series forecasting. This study focuses on assessing load composition at given time of the day according to P, Q, and V sets at that time, rather than predicting load or load composition in the future, i.e., the trained ANN responses are based only on a current input. Therefore, the one-time training of ANN is selected in this paper.

As the one-time training process considers all combinations of voltages and weighting factors, once trained, the ANN can be applied to extract the load compositions at any time of any day in the future, as long as the measurement of bus voltages and the demand are available. Therefore, a robust and accurate training algorithm is required, although it does not have

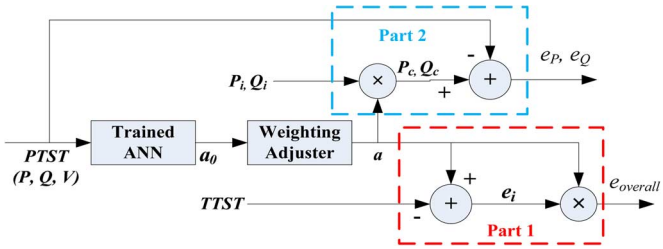

Fig. 5. Validation process block diagram.

to be very fast. According to the description in Section II-B3, BRBP with high accuracy and high robustness is adopted as the training algorithm in this study. Other parameters are configured as a MATLAB default value because their effects are not as significant as parameters mentioned above [17]. The ANN trained in this way captures the relationship among the load supply voltage, load consumption, and the load compositions and the relationship can be used for validation and further application.

D. Validation

1) Validation Data Generation: Similar process for training data generation as described in Section IV-B1–Section IV-B4 is implemented for validation data generation. The input and the target in the validation process can be written as an input matrix ***PTST*** according to (9) and a target matrix ***TTST*** according to (10). The target for validation process is used as a standard to assess the performance of the trained ANN.

2) Validation Process: The block diagram of the validation process is shown in Fig. 5. It consists of two parts: 1) validation of load composition weighting factor (Part 1) and 2) validation of load model (P and Q) calculated by ANN computed composition weighting factors and the individual P and Q consumption (Part 2).

At the beginning, the input data ***PTST*** ($P\&Q\&V$ or $P\&V$) is processed by the trained ANN to create an output vector $\boldsymbol{a_0}$, which contains weighting factors for individual load categories computed by the trained ANN. Due to the error produced during the computation process, the sum of elements inside $\boldsymbol{a_0}$ deviates slightly from 1. To ensure the sum of the weighting factors is exactly equal to 1, a weighting adjuster is installed after the trained ANN to normalize $\boldsymbol{a_0}$. The normalization process is represented as

$$a_i = \frac{a_{0i}}{\sum_{i=1}^{N} a_{0i}} \tag{11}$$

where a_i is the adjusted weighting factor for load category i, a_{0i} is the weighting factor for load category i before adjusting, N is the number of elements in vector $\boldsymbol{a}$ and $\boldsymbol{a_0}$. Therefore, the weighting adjuster output, vector $\boldsymbol{a}$, is regarded as the final computed weighting factors.

a) Weighting factor validation: In Part 1, the weighting adjuster output is compared with the target ***TTST***, the initial weighting factors used to generate ***PTST***. The weighting factor error (WFE) for different individual load categories, Vector $\boldsymbol{e_j}$ in Fig. 5, is obtained by taking the absolute difference between $\boldsymbol{a}$ and ***TTST***. To obtain the overall error ($e_{overall}$) of the disaggregation approach, an aggregation approach is needed to combine the errors of different load categories into an aggregate error. In [23], series of probability combination approaches are proposed, such as average or weighted average, multiplicative average, Bayesian approaches. It is concluded that simple average or weighted average can work better on probability combination problem than more complicated rules which always induce abundant computation tasks and over-performance. As a result, considering the effects of the weights of different load categories on the error aggregation process, weighted average approach is adopted to aggregate individual errors into an overall error, shown as

$$e_{\text{overall}} = \sum_{i=1}^{N} a_i e_i \tag{12}$$

where N is the total number of load categories, $\boldsymbol{a}_i$ is the computed weighting factor for load category i, e_i is the weighting factor estimation error for load category i in each Vector $\boldsymbol{e_j}$, $e_{overall}$ is the aggregate load disaggregation error.

b) Load model validation: In Part 2 of Fig. 5, the computed weighting factors are used to calculate the total real and reactive power at the bulk supply point (P_c, Q_c) with (7). The calculated P and Q, P_c and Q_c, respectively, are compared with the ANN input real and reactive power, and the absolute difference between them, e_P given by

$$e_P = \left| \sum_{i=1}^{N} P_0 \left(\frac{V}{V_0} \right)^{\alpha_i} (a_i - w_i) \right| = P_0 \left| \sum_{i=1}^{N} \left(\frac{V}{V_0} \right)^{\alpha_i} \Delta w_i \right| \tag{13}$$

and e_Q given by

$$e_Q = P_0 \left| \sum_{i=1}^{N} \sqrt{\left(\frac{1}{pf_{0i}} \right)^2 - 1} \cdot \left(\frac{V}{V_0} \right)^{\beta_i} \Delta w_i \right| \tag{14}$$

are defined as corresponding load model error (LME), where N is the total number of load categories, w_i is the weighting factor for load category i used to calculate P and Q in ***PTST***, a_i is the computed weighting factor for load category i, and pf_{0i} is the nominal power factor of load category i.

E. Probabilistic Distribution, Confidence Interval, and Confidence Level of the Errors

As ***PTST*** contains large numbers of randomly generated validation data, both weighting factor errors and load model errors are probabilistically distributed. Thus, probability distribution function (PDF) is adopted to present the distribution of the errors. The confidence interval and the confidence level of the error indicate the reliability of the load disaggregation approach. Confidence interval (CI) is an observed interval that frequently includes the parameter of interest if the experiment is repeated, and confidence level (CL) is defined as the proportion of a confidence interval that contains the true value of the parameter if the confidence level is constructed across many separate data analyses of repeated experiments [24]. To assess the reliability, cumulative distribution function (CDF) is adopted to obtain the confidence levels in different confidence intervals of the errors.

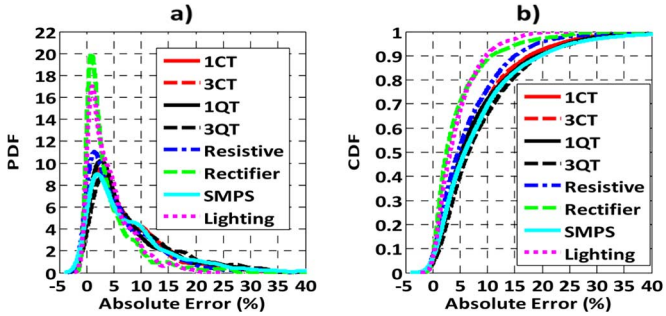

Fig. 6. (a) PDF and (b) CDF of absolute error for individual load categories.

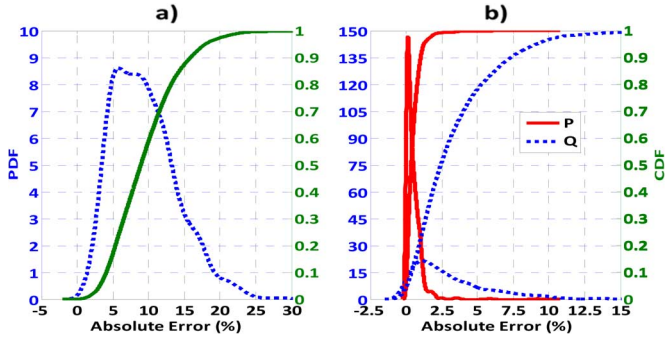

Fig. 7. PDF and CDF of (a) WFEs for the disaggregation approach and (b) P and Q LME, with $P\&Q\&V$ measurement available.

V. Results and Discussion

In this study, there are 8400 $P\&Q\&V$ data sets for training and 2100 $P\&Q\&V$ sets for validation. Implemented in MATLAB 2011a on an Intel(R) Core (TM) i5-2400 CPU @ 3.10GHz computer installed with 32-bit Windows XP system, the training process takes about ten minutes, and the validation process takes up to 1 s. The estimation error of both weighting factors and load models are presented and discussed in this section. Furthermore, the cases with only $P\&V$ measurement available are implemented and compared with the cases with $P\&Q\&V$ measurement available.

A. WFE With P&Q&V Measurement Available

1) WFE of Individual Load Categories: Fig. 6 shows the PDF and CDF of WFE for individual load categories. From the PDF, it can be seen that the most probable WFE (WFE with highest probability density) for all individual load categories ranges from 0% to 5%. The CLs in different error intervals could be read from the data cursor of the CDF. It shows that the CLs for all individual load categories are from 40% to 70% in the error CI [0%, 5%] (i.e., error less than or equal to 5%), from 65% to 90% in the CI [0%,10%], and from 80% to about 97% in the CI [0%, 15%].

2) Overall WFE of the Disaggregation Approach: PDFs or CDFs for different load categories need to be aggregated to an overall PDF or CDF to assess the performance of the disaggregation approach via weighted average process mentioned as (12). However, the most probable WFEs for all individual load categories are not likely to occur simultaneously. In other words, the WFEs of different load categories for each $P\&Q\&V$ input set are probably correlated. Considering this possible circumstance, the probability aggregation process is implemented for every $P\&Q\&V$ set immediately after WFE of each individual load category is obtained ($\boldsymbol{e_i}$ in Part 1, Fig. 5), rather than after PDFs and CDFs for all individual load categories are produced.

Fig. 7(a) shows aggregate PDF and CDF of the WFE for the load disaggregation approach. From PDF, it is observed that the error is most likely to be about 6%. On the data cursor of CDF, it can be read that the confidence level of the disaggregation approach is about 20% in the confidence interval [0%, 5%], 60% in the CI [0%, 10%], and 90% in the CI [0, 15%]. In other words, for every $P\&Q\&V$ measurement set, the error of the load disaggregation approach is less than 15% in 90% of the case, less than 10% in 60% of the cases.

By comparing CDFs in Fig. 6(b) and Fig. 7(a), it is also observed that at 5% and 10%, the cumulative probability of aggregate WFE is lower than any of the individual WFE. Simultaneously, from PDFs in Fig. 6(a) and Fig. 7(a), it is observed that the most probable value for aggregate WFE falls in interval [5%, 10%] and within [0%, 5%] for any of the individual WFE. These verify the consideration of correlations among different WFEs, justify the error aggregation for every input set immediately after the WFs and WFEs are computed, and repudiate the routine of individual PDF and CDF aggregation, all discussed in Section IV-D2a.

B. Load Model Error (LME) With P&Q&V Measurement Available

Fig. 7(b) shows the PDFs and CDFs of P and Q load model errors (LMEs). From PDF, the LME with highest probability density occurs at about 0.13% for P and 1% for Q. From the data cursor in CDF it can be seen that P LME is less than 1% in over 90% of the cases. While Q LME is less than 7.5%, in over 90% of the cases, i.e., Q LME is more affected by weighting factor deviations than P LME. This can be explained with the sensitivity of the LME to the WFE. From (13) and (14), the complete differential of e_P and e_Q at Point $(\Delta w_1, \ldots, \Delta w_i, \ldots, \Delta w_N)$ can be written, respectively, as

$$\partial e_P = P_0 \left| \sum_{i=1}^{N} \left(\frac{V}{V_0} \right)^{\alpha_i} \partial \Delta w_i \right| \tag{15}$$

$$\partial e_Q = P_0 \left| \sum_{i=1}^{N} \sqrt{\left(\frac{1}{pf_{0i}} \right)^2 - 1} \cdot \left(\frac{V}{V_0} \right)^{\beta_i} \partial \Delta w_i \right| \tag{16}$$

respectively, where Δw_i is the WFE of load category i.

On the one hand, for individual load categories, the absolute value of α is smaller than β under the same voltage, which contributes to the larger sensitivity of Q LME than P LME. On the other hand, when there are a large number of devices with nominal power factor lower than 0.707 (i.e., rectifier with passive power factor correction circuit, some induction motors etc.), the sensitivity of LME of Q to WFE will increase faster, especially when the actual voltage is higher than 1p.u and when the WFE for these individual load categories are positive. However, when the WFE of some individual load categories are negative and their sensitivities are relatively large, the Q LME could be smaller than P LME. Fig. 8 shows that most of the points

(e_{Pi}, e_{Qi}) fall above the line $e_Q = e_P$. In other words, P LME is smaller than Q LME in most cases.

Compared with Fig. 7(a), Fig. 7(b) also shows that in the same confidence interval, LME has noticeably higher confidence level than WFE. This means that the variation in load composition estimation does not significantly affect the estimation of aggregate load characteristic.

C. LME With P&V Measurement Available

In some cases, Q rms measurement is not available (Case 2). The result for both WFE and P LME in this case is obtained as well and compared with the case when $P\&Q\&V$ are all available (Case 1). The rules of ANN parameter configuration, the ANN training algorithm, the training data and the testing data (apart from Q) in both cases are exactly the same. The PDFs and CDFs of aggregate WFE and P LME under both cases are shown in Fig. 9(a) qand (b), respectively. The most probable values of both WFE and P LME are smaller in Case 1 than in Case 2. The confidence levels within the same confidence interval, for both aggregate WFE and P LME are higher in Case 1 than in Case 2. The visible difference between the two cases shows that the ANN will perform the disaggregation approach better with all $P\&Q\&V$ rms measurement available than with only P&V available. It can be inferred that for $P\&V$ input only there is large number of possible combinations of different load compositions that can describe the $P-V$ relationship, while the addition of Q measurement narrows the range of the possibilities as it determines the power factor of the total load and the approximate participation of different load categories. Therefore, Q plays a significant role in the ANN-based load disaggregation approach.

VI. Conclusion

Considering the voltage-dependent characteristics of the substation load, an AI-based real-time load disaggregation approach is developed, in which only the substation P, Q and V rms measurements are needed. The approach makes use of the relationship among the load supply voltage, load composition and the load consumptions, and employs ANN to capture such relationships and save it as a tool. Once developed, with $P\&Q\&V$ measurement from the substation, the tool can work out the percentage of different load categories, with certain confidence levels for different disaggregation error intervals. Furthermore, the obtained load composition can be used to estimate the P and Q load characteristics via component-based load modeling approach, with high confidence levels for different load model error intervals.

From the result presented in the paper, it can be concluded that the deviation of load composition will not dramatically affect the load characteristics, especially real power characteristics. Simultaneously, with the identical parameter setting rules and the training algorithm of the ANN, the case with only $P\&V$ rms measurement available performs less accurately than the case with $P\&Q\&V$. This indicates the significant role of reactive power measurement for load disaggregation approach.

The proposed approach can contribute to the real time estimation of different customer energy consumption at the bulk supply point without direct or indirect contact with the customers and the real time estimation of dynamic load characteristics at the bulk supply point without voltage disturbance experiments. It can provide suggestions on DSM, renewable device installation, and help close to real-time control. Furthermore, with supplementary weather information [25] and past energy consumption data and by adopting load forecasting tools (e.g., AI-based), the presented approach can be used to predict the consumptions of different load categories in advance (e.g., hours or days), which helps real-time electricity price regulation and customer energy consumption plan.

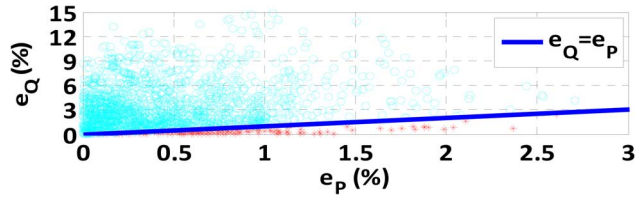

Fig. 8. $e_P - e_Q$ plot against Line $e_Q = e_P$.

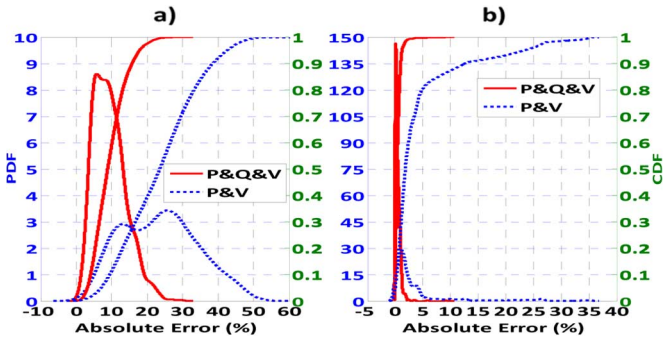

Fig. 9. (a) Aggregate WEF comparison PDF and CDF for both cases. (b) Real power LME comparison PDF and CDF.

References

[1] Intertek, "R66141 Household Electricity Survey_A Study of Domestic Electrical Product Usage," 2012.
[2] S. Hesmondhalgh, "GB Energy Demand-2010 and 2025 Initial Brattle Electricity Demand-Side Model-Scope for Demand Reduction and Flexible Response," 2012.
[3] R. Stamminger and R. Friedrich-Wilhelms, *Synergy Potential of Smart Appliances*. Bonn, Germany: Univ. Bonn, 2008.
[4] L. Jian, S. Ng, G. Kendall, and J. Cheng, "Load signature study—Part I: Basic concept, structure, methodology," *IEEE Trans. Power Del.*, vol. 25, no. 2, pp. 551–560, Apr. 2010.
[5] M. Figueiredo, A. de Almeida, and B. Ribeiro, "Home electrical signal disaggregation for non-intrusive load monitoring (NILM) systems," *Neurocomputing*, vol. 96, pp. 66–73, 2012.
[6] H. Yan, Z. Zabar, D. Czarkowski, L. Birenbaum, E. Levi, and J. Hajagos, "Experimental test of a load model in the presence of harmonics," *Proc. Inst. Electr. Eng.—Gener., Transm. Distrib.*, vol. 146, pp. 186–192, 1999.
[7] C. Cresswell, S. Djokic, K. Ochije, and E. Macpherson, "Modelling of non-linear electronic loads for power system studies: A qualitative approach," presented at the 19th Int. Conf. Electricity Distribution, 2007.
[8] C. Cresswell and S. Djokic, "Representation of directly connected and drive-controlled induction motors. Part 1: Single-phase load models," in *Proc. 18th Int. Conf. Electrical Mach.*, 2008, pp. 1–6.
[9] C. Cresswell and S. Djokic, "Representation of directly connected and drive-controlled induction motors. Part 2: Three-phase load models," in *Proc. 18th Int. Conf. Electrical Mach.*, 2008, pp. 1–6.
[10] C. Cresswell and S. Djokic, "Steady-state models of low energy consumption light sources," presented at the 16th Power Syst. Computation Conf., 2008.

[11] CIGRE Working Group C4.605, Rep.5, "Modelling and Aggregation of Loads in Flexible Power Networks," (566), Feb. 2014.
[12] H. Ku-Long, Y.-Y. Hsu, and Y. Chien-Chuen, "Short term load forecasting using a multilayer neural network with an adaptive learning algorithm," *IEEE Trans. Power Syst.*, vol. 7, no. 1, pp. 141–149, Feb. 1992.
[13] A. Khotanzad, R. Afkhami-Rohani, T. L. Lu, A. Abaye, M. Davis, and D. J. Maratukulam, "ANNSTLF-a neural-network-based electric load forecasting system," *IEEE Trans. Neural Netw.*, vol. 8, no. 4, pp. 835–846, 1997.
[14] T. Hong, P. Pinson, and S. Fan, "Global energy forecasting competition 2012," *Iint. J. Forecasting*, vol. 30, no. 2, pp. 357–363, 2012.
[15] G. Chicco, R. Napoli, and F. Piglione, "Comparisons among clustering techniques for electricity customer classification," *IEEE Trans. Power Syst.*, vol. 21, no. 2, pp. 933–940, May 2006.
[16] L. Du, D. HE, Y. Yang, J. A. Restrepo, B. Lu, R. G. Harley, and T. G. Habetler, "Self-organizing classification and identification of miscellaneous electric loads," in *Proc. IEEE PES Gen. Meeting*, San Diego, CA, USA, 2012, pp. 1–6.
[17] H. Demuth, M. Beale, and M. Hagan, MATLAB Neural Network Tookbox User's Guide. H. Demuth, M. Beale, and M. Hagan, Eds., 2009.
[18] K. Gurney*, An Introduction to Neural Network*. London, U.K.: Univ. College London, 1997.
[19] S. Xu and L. Chen, "A novel approach for determining the optimal number of hidden layer neurons for FNN's and its application in data mining," in *Proc. 5th ICITA*, 2008, pp. 683–686.
[20] Y. Liu, J. A. Starzyk, and Z. Zhu, "Optimizing number of hidden neurons in neural network," in *Proc. 25th IASTED Int. Multi-Conf.: Artif. Intell. Applications*, 2007, pp. 121–126.
[21] I. Ileanć, C. Rotar, and A. Incze, "The optimization of feed forward neural networks structure using genetic algorithms," in *Proc. ICTAMI*, Thessalonili, Greece, 2004, pp. 223–230.
[22] J. V. Milanović, K. Yamashita, S. M. Villanueva, S. Ž. Djokić, and L. M. Korunović, "International industry practice on power system load modelling," *IEEE Trans. Power Syst.*, vol. 28, no. 4, pp. 3038–3046, Nov. 2013.
[23] R. T. Clemen and R. L. Winkler, "Combining probability distributions from experts in risk analysis," *Risk Analysis*, vol. 19, pp. 187–203, 1999.
[24] J. Sheng, S. Xie, and C. Pan*, Probability Theory and Mathematical Statistics*, 4th ed. Beijing: Higher Education Press, 2008.
[25] Weather History@Weather.org [Online]. Available: http://weather.org/weatherorg_records_and_averages.htm

Yizheng Xu (S'12) received the B.S. degree in electrical and electronic engineering from the University of Manchester, Manchester, U.K. and North China Electric Power University, Beijing, China, in 2011. She is currently working toward the Ph.D. degree at the University of Manchester.

Jovica V. Milanović (M'95–SM'98–F'10) received the Dipl.Ing. and M.Sc. degrees from the University of Belgrade, Belgrade, Yugoslavia, the Ph.D. degree from the University of Newcastle, Newcastle, Australia, and the D.Sc. degree from the University of Manchester, Manchester, U.K., all in electrical engineering.

He is currently a Professor of electrical power engineering, Deputy Head of the School of Electrical and Electronic Engineering, and Head of Electrical Energy and Power Systems Group of the University of Manchester, Manchester, U.K., a Visiting Professor with the University of Novi Sad, Novi Sad, Serbia, and a Conjoint Professor with the University of Newcastle, Newcastle, Australia.